



Synthesis and characterization of porous monodisperse carbon spheres/selenium composite for high-performance rechargeable Li–Se batteries

Jun YAN^{1,2}, Wei-fang LIU¹, Cheng CHEN¹, Chen-hao ZHAO³, Kai-yu LIU^{1,2}

1. School of Chemistry and Chemical Engineering, Central South University, Changsha 410083, China;

2. Hunan Provincial Key Laboratory of Efficient and Clean Utilization of Manganese Resources, Central South University, Changsha 410083, China;

3. College of Chemistry and Materials Science, Longyan University, Longyan 364000, China

Received 17 June 2017; accepted 12 December 2017

Abstract: In order to find the appropriate material to load selenium for higher performance of rechargeable Li–Se batteries, the resorcinol–formaldehyde resins derived monodisperse carbon spheres (RFCS)/Se composites were fabricated by the melting–diffusion method. The RFCS were obtained from initial carbonization of resorcinol–formaldehyde resins and subsequent KOH activation. Three kinds of samples of the RFCS/Se composites with different mass ratios were characterized by XRD, Raman spectroscopy, SEM, BET and EDS tests, which demonstrate that the samples with diverse mass fractions of selenium have distinct interior structure. The most suitable RFCS/Se composite is found to be the RFCS/Se-50 composite, which delivers a high reversible capacity of 643.9 mA·h/g after 100 cycles at current density of 0.2C.

Key words: lithium–selenium batteries; cathode material; carbon sphere; sol–gel process

1 Introduction

There have always been urgent demands for rechargeable lithium-ion batteries due to the increasing consumption of various technological applications including portable electronic devices, energy storage and electric vehicles. In the last decades, the lithium-ion batteries with higher energy density were still hindered by the high-performance cathode materials [1–3]. Sulfur has been considered as potential cathode material for the lithium-ion batteries owing to its superior theoretical specific capacity (1675 mA·h/g), with which a high energy density (2600 W·h/kg) can be reached [4]. However, lithium–sulfur batteries which consist of sulfur are plagued with two major problems that sulfur is highly electric/ionic insulating and polysulfides are soluble in electrolytes during discharge–charge process [4–6].

Recently, extensive studies have been carried out on selenium which belongs to the same family as sulfur [7–10]. Notably, selenium has a much higher

electrical conductivity of 1×10^{-3} S/m than sulfur (5×10^{-28} S/m) which is beneficial for faster transport of Li^+ ion and higher utilization of the active cathode material. Though Se owns a lower theoretical gravimetric capacity (678 mA·h/g) than S (1675 mA·h/g), its higher density compensates for the deflection and offers a high theoretical volumetric capacity (3253 mA·h/cm), compared to that of S (3467 mA·h/cm) [11,12]. All these merits mentioned above indicate that Se can be regarded as a promising cathode material for high-performance lithium-ion batteries.

Similar to Li–S batteries, Li–Se batteries also suffer from the intractable issues mainly involving relatively low electric conductivity and dissolution of polyselenide intermediates, which result in low Coulombic efficiency and poor cycling stability [7,13–15]. To overcome the intrinsic issues, one of the effective strategies is to confine selenium and polyselenides into special carbonaceous materials which have high specific surface area, appropriate pore size and specific morphology.

Foundation item: Project (21471162) supported by the National Natural Science Foundation of China; Project supported by the Recruitment Program of Global Youth Experts, China; Project (20130162120031) supported by Research Fund for the Doctoral Program of Higher Education of China

Corresponding author: Jun YAN, Tel: +86-13135289306, E-mail: yanjun@csu.edu.cn; Kai-yu LIU, Tel: +86-13548590751, E-mail: kaiyuliu309@163.com
DOI: 10.1016/S1003-6326(18)64826-5

Herein, we present a strategy to fabricate resorcinol–formaldehyde resins derived monodisperse carbon spheres (RFCS), and the C/Se composite can be obtained using above RFCS as the substrate. The obtained RFCS possesses a uniform polyporous structure with numerous surface micropores which can be served as sites to load Se. Hence, the spherical carbon framework can provide an effective and stable structure during cycling. Also, the variation of electrochemical performances induced by different contents of Se in the composite are explored. As a result, the RFCS/Se composites have been fabricated to enhance the comprehension of design and synthesis in cathode materials for Li-ion batteries.

2 Experimental

2.1 Materials preparation

2.1.1 Synthesis of RFCS

The resorcinol–formaldehyde resins derived monodisperse spheres (RFCS) were synthesized through the sol–gel process which is analogous to the Stöber method [16]. In detail, a solution composed of 0.3 mL ammonia solution (25%, mass fraction), 60 mL deionized water and 24 mL absolute ethanol was firstly prepared and stirred for 30 min. Subsequently, 0.45 g resorcinol and 0.63 mL formaldehyde solution (~37%, mass fraction) were added. Then, after continuous stirring at room temperature for 24 h, the solution was held at 100 °C for 24 h in a Teflon-lined stainless steel autoclave. The RFCS were collected through the centrifugation of the aforementioned solution and then dried at 80 °C for 6 h. The carbonization process of RFCS were further conducted under nitrogen atmosphere at 600 °C for 4 h and then cooled to room temperature naturally.

2.1.2 KOH chemical activation of RFCS

The obtained RFCS were added into KOH solution (RFCS:KOH=1:3, in mass ratio), and the mixture was stirred for 30 min. Then, the wet compound was dried at 100 °C, followed by a heat treatment at 650 °C for 30 min under the protection of argon. The activated RFCS were then filtered and washed using 1 mol/L hydrochloric acid and deionized water thoroughly until the pH reached neutral, and then dried at 100 °C overnight.

2.1.3 Preparation of RFCS/Se composite

RFCS/Se composite was prepared by a melting diffusion method. Firstly, selenium powder and the activated RFCS were mixed and ground in anagate mortar with different mass ratios of RFCS to Se (5:5, 4:6 and 3:7) to investigate the impact of Se content on their electrochemical performances. The samples were distinguished as RFCS/Se-50, RFCS/Se-60 and RFCS/Se-70. Next, the mixture was moved to corundum

porcelain and heated at 260 °C in argon atmosphere for 6 h.

2.2 Material characterization

The surface structures, morphologies and elements mapping were analyzed by JEOL JSM–7500F field-emission scanning electron microscope (FESEM, 5 kV). TEM and HRTEM images were collected on a Tecnai-G20 transmission electron microscope operating at an accelerating voltage of 200 kV. The nitrogen adsorption/desorption curves were recorded on a Micromeritics (USA) gas adsorption/desorption instrument at 77 K. XRD characterization was measured using a powder X-ray diffractometer (DX–2700, Dandong) with Cu K α radiation (35 kV, 30 mA) and 0.04 (°)/s in the 2 θ range between 10° and 80°. Analysis of surface elements was conducted by X-ray photoelectron spectroscopy (XPS) using a twin-anode Al K α (1486.6 eV) X-ray source. Thermogravimetric analysis (TGA; STA 449 F3 Jupiter, Netzsch, Germany) was conducted from 20 to 800 °C at a heating rate of 5 °C/min in argon atmosphere to determine the true selenium content of various RFCS/Se composites. The Raman spectrum (RenishawVia 2000) was recorded at the fixed wavelength of 514.5 nm to study the structure of the samples.

2.3 Electrochemical measurements

CR 2016 coin cells were used throughout the experiments to evaluate the electrochemical performance of various RFCS/Se composite. The working electrode was prepared as follows. Firstly, RFCS/Se composite, super P carbon black and sodium alginate were mixed at the mass ratio of 7:2:1 in deionized water to form the slurry. Then, the slurry was coated on aluminum foil and evaporated completely at 80 °C overnight. At last, the coated aluminum foil was punched into circular electrodes with a diameter of 14 mm. Besides the working electrode, the half cell consists of a Celgard 2400 film used as the separation and commercial LBC 301 LiPF $_6$ solution (Shenzhen CAPCHEM) as electrolyte, which was assembled in an argon filled glove box. Cyclic voltammetry (CV) measurements were tested with a Modula XM electrochemical measurement system (Solartron, UK) at a scan rate of 0.1 mV/s within 1.0–3.0 V (vs Li/Li $^+$). Galvanostatic measurements were conducted on a battery test system (Neware CT–3008) at different current densities within a voltage range of 1.0–3.0 V at room temperature.

3 Results and discussion

The synthesis procedure of RFCS/Se composite is schematically illustrated in Fig. 1. The resorcinol and

formaldehyde were firstly added into the mixture of water and alcohol with ammonia as a catalyst. After stirring for 24 h at room temperature, the solution was transferred in a Teflon-lined stainless steel autoclave through hydrothermal treatment. The obtained solid polymer was then collected for further carbonization and activation. Finally, the RFCS were mixed with selenium

and heated at 260 °C under argon protection, and then RFCS/Se composite was obtained.

The XRD patterns of pristine selenium, RFCS and RFCS/Se composites with different mass ratios of selenium are shown in Fig. 2(a). As for RFCS, the broad peak nearby $2\theta=24^\circ$ indicates an amorphous state of carbon material. In comparison, the XRD pattern of

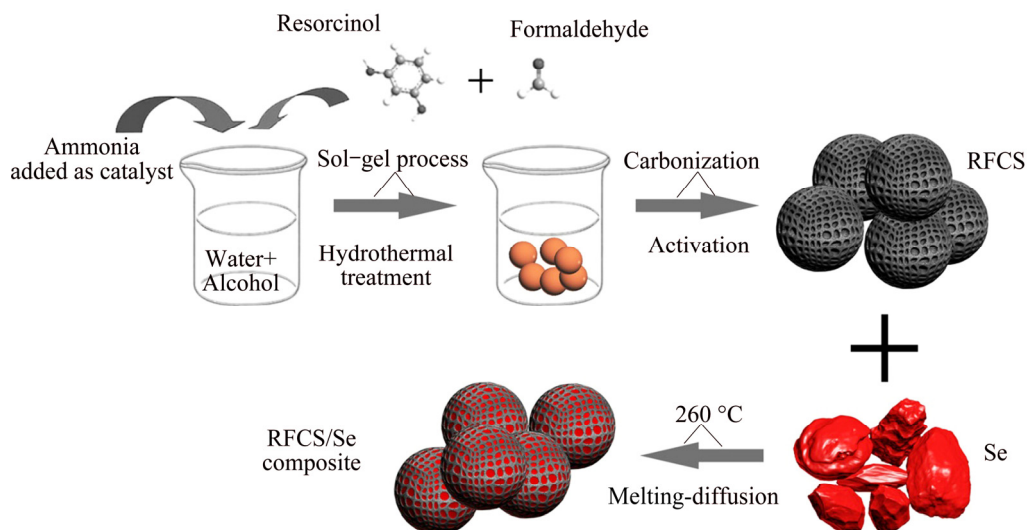


Fig. 1 Detailed synthesis route of RFCS/Se composite

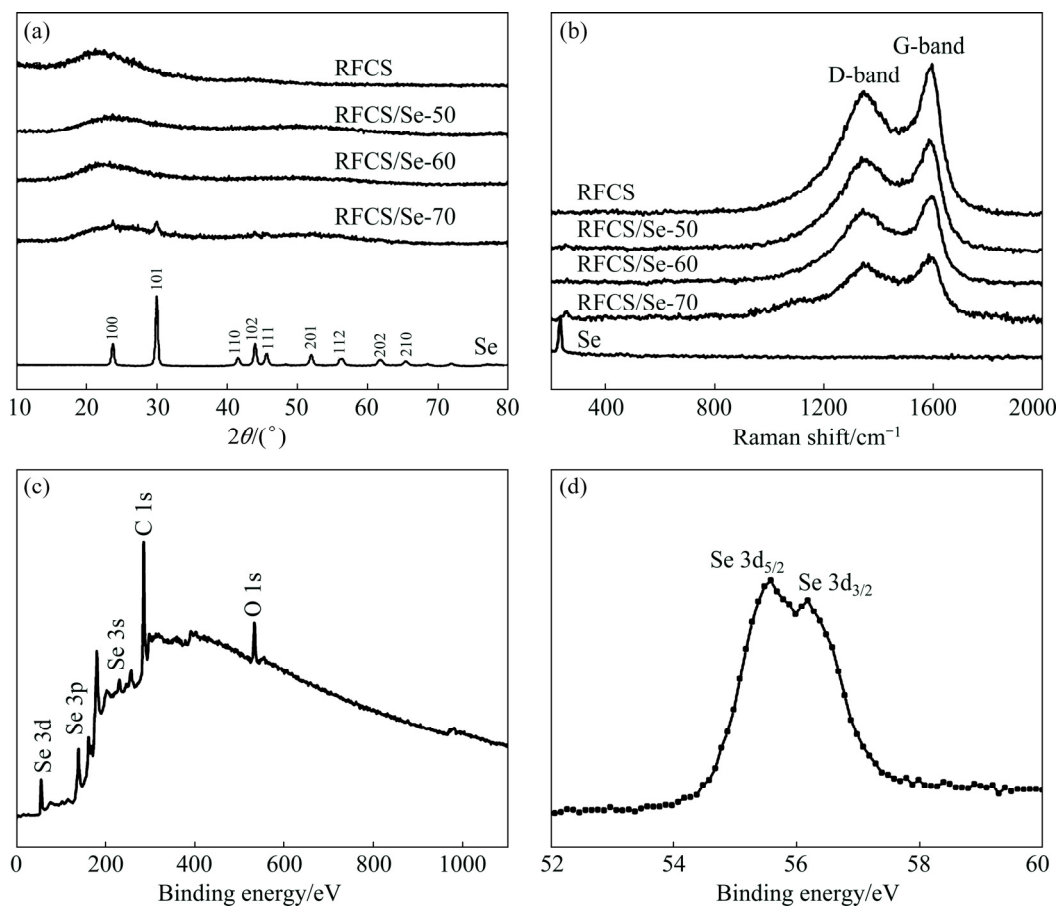


Fig. 2 XRD patterns (a) and Raman spectra (b) of Se, RFCS and RFCS/Se composites, XPS spectrum of RFCS/Se-50 composite (c), and high-resolution spectrum of Se 3d for RFCS/Se composite (d)

RFCS/Se-50 and RFCS/Se-60 composite is similar to that of RFCS. Obviously, all the sharp diffraction peaks of selenium disappear entirely after the formation of RFCS/Se composite, indicating the dispersion of selenium at an atomic or molecular level in the obtained RFCS. However, some diffraction peaks of Se can be observed in RFCS/Se-70 composite, suggesting that the excessive Se with a crystalline state cannot enter the porous structure of RFCS. The structural features of pristine selenium, RFCS and RFCS/Se composites with different mass ratios are further investigated by Raman spectroscopy (Fig. 2(b)). The peak at $\sim 1350\text{ cm}^{-1}$ represents disordered carbon (D band), and the peak at $\sim 1580\text{ cm}^{-1}$ corresponds to the graphitic carbon (G band), revealing the partially graphitized nature of the obtained RFCS [17]. For the pristine selenium, there is a single peak located at 235 cm^{-1} . Interestingly, this characteristic peak disappears while Se is infused into the RFCS except for the RFCS/Se-70 composite with excessive Se in crystalline state. Raman and XRD measurements both

confirm that Se is encapsulated in RFCS to form an amorphous structure.

In order to explore the chemical bonding state and surface chemical composition of the RFCS/Se composite, the XPS measurements of the RFCS/Se-50 composite are conducted. Figure 2(c) depicts several peaks in the XPS survey spectra of RFCS/Se-50 composite. Peaks located at ~ 56.1 , ~ 162.1 and $\sim 231.1\text{ eV}$ correspond to Se 3d, Se 3p and Se 3s, respectively. The peaks at ~ 284.5 and $\sim 533.5\text{ eV}$ correspond to C 1s and O 1s, respectively. These results verify the co-existence of Se, C and O elements in the RFCS/Se composite. In the Se 3d spectrum (Fig. 2(d)), two peaks located at 55.4 and 56.2 eV correspond to Se $3d_{5/2}$ and Se $3d_{3/2}$, respectively, which are ascribed to spin-orbit coupling [18].

The FESEM images of the RFCS and RFCS/Se composites with different mass ratios are revealed in Fig. 3. In Fig. 3(a), the RFCS are self-assembled from the sol-gel process of resorcinol-formaldehyde resins and further carbonization, which present regular

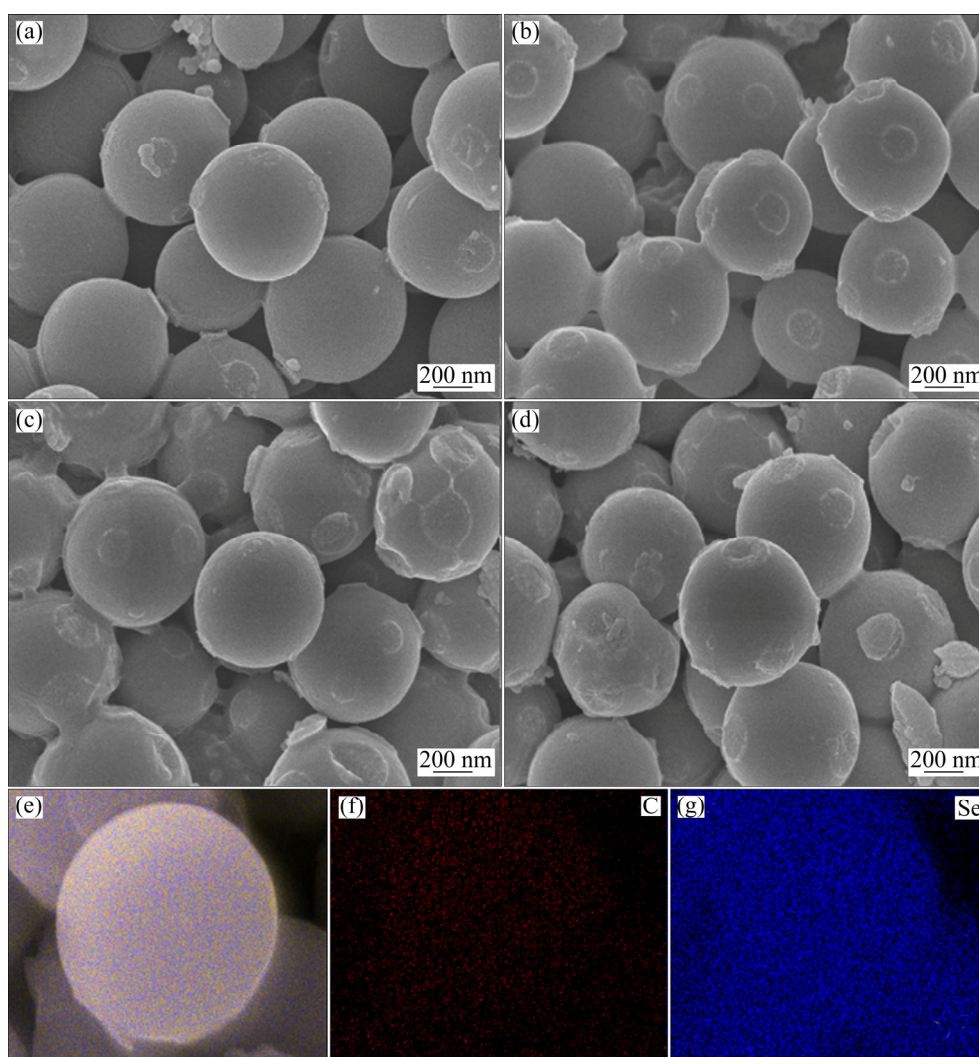


Fig. 3 FESEM images of RFCS (a), RFCS/Se-50 (b), RFCS/Se-60 (c) and RFCS/Se-70 (d) composites, and EDS mapping of RFCS/Se-50 composite showing distribution of all elements (e), carbon (f) and selenium (g)

spherical shape and excellent uniformity with an average diameter of 500 nm. Figures 3(b) and 3(c) present the morphologies of the RFCS/Se-50 and RFCS/Se-60 composite, respectively, in which Se is uniformly distributed after the heat treatment. However, the morphology of RFCS/Se-70 composite with the highest content of Se (Fig. 3(d)) shows the difference from that of RFCS/Se-50 and RFCS/Se-60 composites, and partial bulk crystalline Se can be observed. The result is in good agreement with the XRD pattern of the RFCS/Se-70 composite in which the partial crystalline Se exists. The EDS mapping (Figs. 3(e–g)) of the RFCS/Se-50 composite describes the good distribution of Se. From Fig. 3(g), it is obvious that the carbon spheres absorb selenium neatly, confirming that selenium is highly dispersed in RFCS.

The pore size distribution and specific surface area of the RFCS and RFCS/Se composites were studied by nitrogen adsorption/desorption isotherms. After the formation of composite, the specific surface area of RFCS/Se composite decreases dramatically from 1705.1 m²/g for RFCS to 28.9 m²/g for RFCS/Se-50 composite, revealing that Se fills in the pores of the RFCS. Moreover, the sharp drop in pore volume from 0.783 to 0.023 cm³/g confirms again that Se is enclosed in the small pores of the RFCS (Fig. 4(a)). The RFCS/Se-60 and RFCS/Se-70 composites exhibit a specific surface area of 7.7 and 5.7 m²/g with pore volume of 0.011 and 0.007 cm³/g, respectively (Fig. 4(b)), and the further decrease in the pore volume can be attributed to the loading of more Se comparatively. The results indicate that all the small pores (with an average diameter of 3.47 nm) are almost filled with amorphous selenium. And the unoccupied pores provide an interspace with the volume variation of Se during the discharge–charge process, especially for RFCS/Se-50 composite.

TEM and HRTEM are operated to further investigate the structural and morphological characteristics of the RFCS and RFCS/Se composites (Fig. 5). It can be observed that RFCS has lots of approximately 3 nm mesopores and abundant micropores (Figs. 5(a, c)). The results are in good accordance with the pore structure pattern shown in Fig. 4(b). After the impregnation of Se, the RFCS/Se-50 composite can retain a smooth surface with a homogeneous distribution for Se (Fig. 5(c)). In comparison with the RFCS sample (Fig. 5(a)), the overall uniform spherical morphology can be maintained after selenium is encapsulated into the RFCS hosts, indicating that almost all the Se is infused into the RFCS instead of coating on the surface. The high resolution TEM image shown in Fig. 5(d) demonstrates the specific micropores of the RFCS/Se-50 composite.

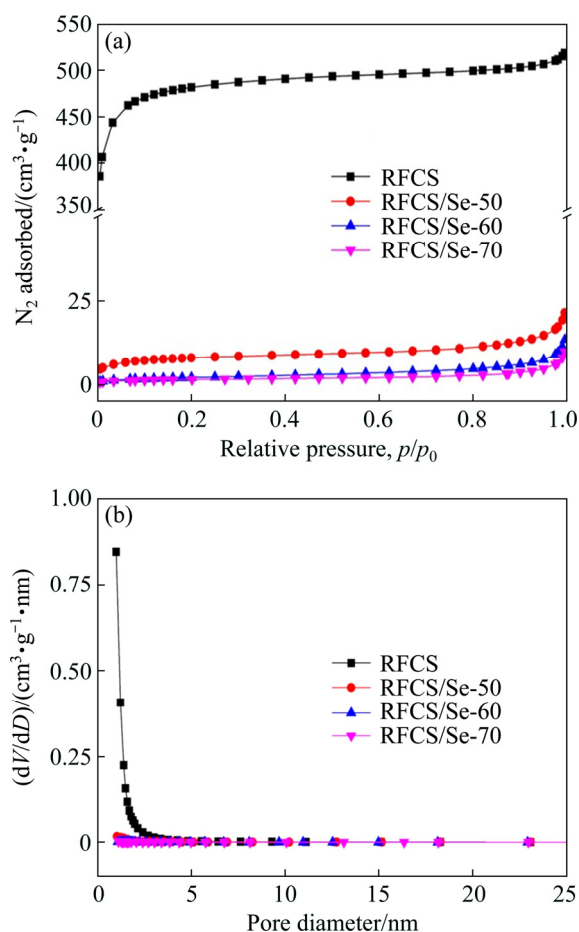


Fig. 4 N₂ adsorption–desorption isotherms (a) and pore size distribution (b) of RFCS and RFCS/Se composite with different mass ratios

These small pores of carbon filled with amorphous selenium can not only immobilize the selenium and polyselenides but also provide sufficient contact area with the electrolyte–carbon interface during electrochemical reaction. The microstructures of RFCS and RFCS/Se-50 composite revealed in Fig. 5 are in good accordance with the results of nitrogen adsorption/desorption isotherms.

To confirm the true content of selenium in the RFCS/Se composite, the samples were analyzed by TGA under an argon atmosphere, and the results are shown in Fig. 6(a). RFCS/Se composites with different mass ratios of selenium are determined to have 38.78%, 49.95% and 63.26% Se. The sharp drop curve of RFCS/Se-50 composite occurring at 200 °C is due to the unoccupied micropores which have absorbed much water naturally. The mass loss of Se may be caused by slight evaporation of Se, according to its melting point of 221 °C. The RFCS/Se composite as a cathode was assembled with Li anode in the half cell, for the testing of electrochemical behaviors. Figure 6(b) shows the cyclic voltammograms (CVs) of the RFCS/Se-50 electrode for the initial three

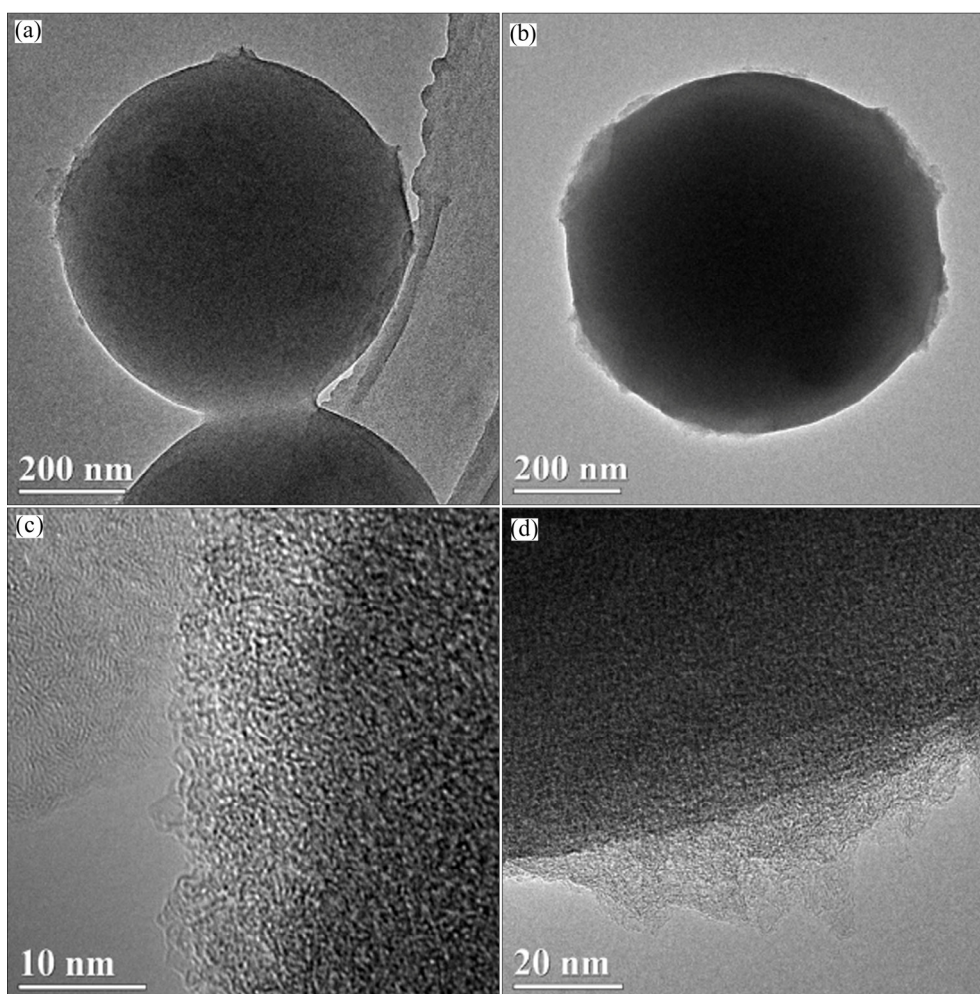


Fig. 5 TEM images (a, b) and HRTEM images (c, d): (a, c) RFCS; (b, d) RFCS/Se-50 composite

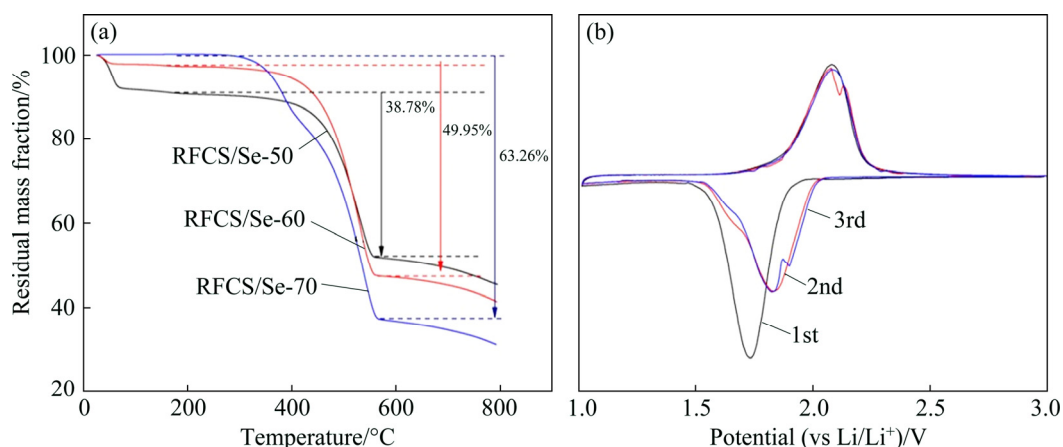


Fig. 6 TGA curves of RFCS/Se composites (a) and CV curves of RFCS/Se-50 electrode at 0.01 mV/s (b)

cycles. In the first discharging curve, a reduction peak located at ~ 1.73 V can be found to correspond to the lithiation of Se. Especially, two separated peaks of reduction at ~ 1.79 and ~ 1.88 V are observed from the third discharging curve. These curves suggest that two kinds of Se molecules react with Li anode, resulting in different voltages [18]. The subsequent CV curves

overlap well with each other, revealing the good cycling stability of the RFCS/Se-50 electrode.

Galvanostatic discharge–charge measurements are conducted in the operating potential range of 1.5–3.0 V (Li/Li^+), and all of the specific capacities are calculated based on true mass of Se in different RFCS/Se composites. Figure 7(a) depicts the discharge–charge

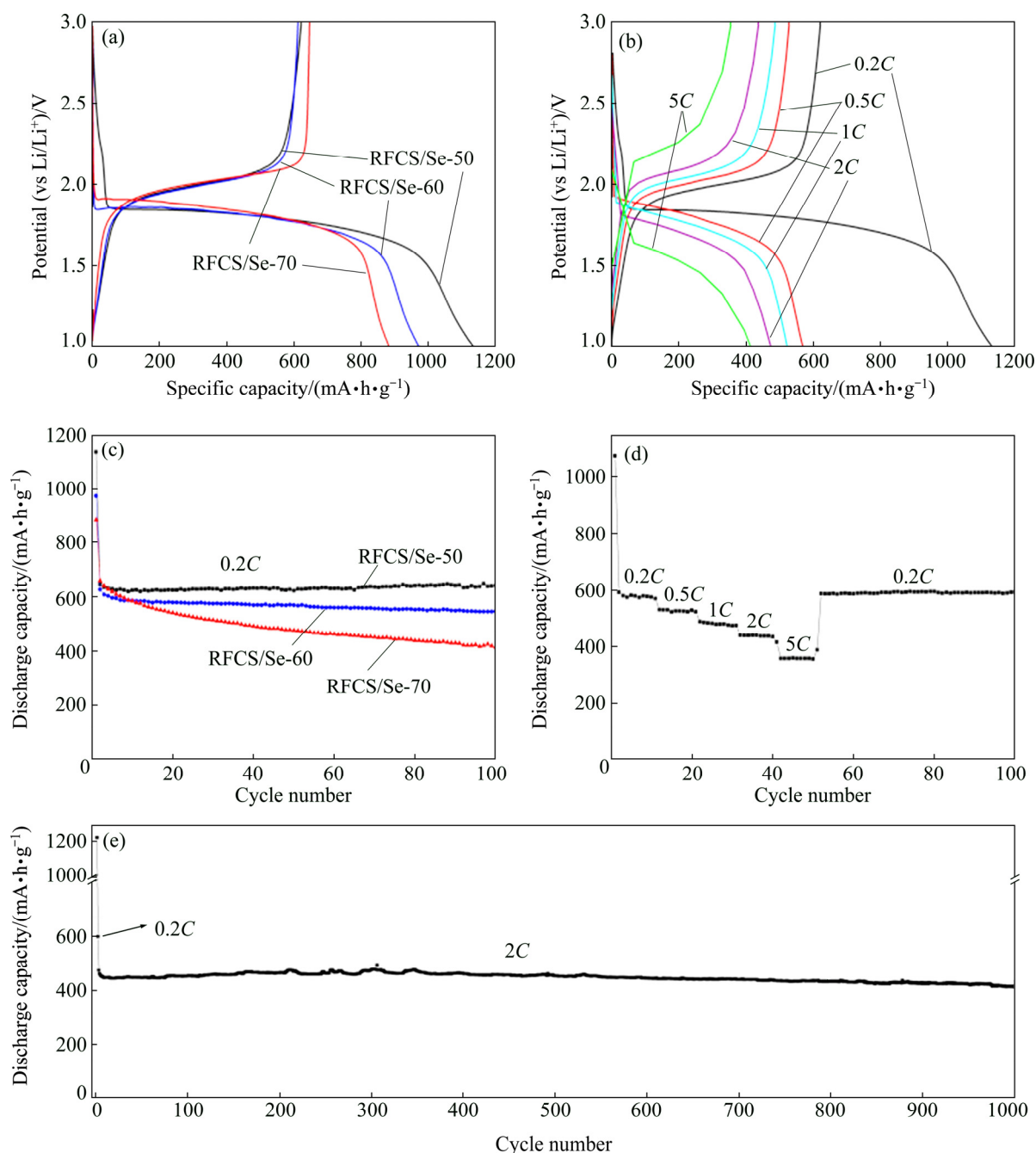


Fig. 7 Discharge–charge profiles of RFCS/Se electrodes at current density of 0.2C (a) and RFCS/Se-50 electrode at different rates (b), cycling performance of RFCS/Se electrodes (c), rate capability of RFCS/Se-50 electrode (d), and 1000-cycle performance of RFCS/Se-50 electrode (e)

profiles for the first cycle of the RFCS/Se-50, RFCS/Se-60 and RFCS/Se-70 composites. As shown, only a single plateau is observed upon the initial discharge process of the RFCS/Se-50, RFCS/Se-60 and RFCS/Se-70 composites with discharge capacity of 1135.1, 957.2 and 883.7 mA·h/g. The discharge plateau of the RFCS/Se-50 and RFCS/Se-60 composite starts at ~1.8 V, while the RFCS/Se-70 composite possesses a higher discharge plateau of ~1.9 V which can be attributed to the crystalline Se [19]. The results are in correspondence with the XRD and FESEM analysis

which shows the existence of crystalline Se in the RFCS/Se-70 composite. During the initial charge process, the electrodes show a reversible capacity of 621.9, 602.4 and 646.2 mA·h/g for RFCS/Se-50, RFCS/Se-60 and RFCS/Se-70 composites, corresponding to the initial Coulombic efficiency of 54.8%, 62.9% and 73.1%, respectively. Compared to the theoretical capacity of Se, the exceeding portion of initial discharge capacity of RFCS/Se composite might be ascribed to the formation of solid–electrolyte interphase (SEI) film [20,21]. Meanwhile, the formation of SEI film is related to the

specific surface area. The material with higher surface area leads to more amount of SEI film. Thus, this outcome is consistent with the results of BET measurements that the RFCS/Se-70 composite with the highest initial Coulombic efficiency possesses the lowest specific area. The discharge–charge profiles of the RFCS/Se-50 electrode at different rates (0.2C, 0.5C, 1C, 2C and 5C) are shown in Fig. 7(b). With the variation of rates from 0.2C to 5C, the charge capacity decreases mildly and the curves of charge plateaus change gradually, illustrating that there is little electrochemical resistance during the discharge–charge process and a high rate capability of RFCS/Se-50 electrode.

Figure 7(c) demonstrates the cycling performance of the RFCS/Se electrodes with different mass ratios. The reversible capacities of RFCS/Se-60 and RFCS/Se-70 electrodes decline to 538.9 and 413.4 mA·h/g, respectively. However, the RFCS/Se-50 electrode has the most stable cycling performance with a reversible capacity of 643.9 mA·h/g after 100 cycles, even higher than the values of initial few cycles, which is due to the continuous activation of Se. The extraordinary cycling performance of the RFCS/Se-50 electrode can be ascribed to the sufficient impregnation of Se and unoccupied small pores which offer a volume for the expansion of Se upon lithiation process. The rate capability of RFCS/Se-50 electrode is depicted in Fig. 7(d). With increasing the rates from 0.2C to 5C, the discharge capacity of RFCS/Se-50 electrode decreases from 592.1 to 358.2 mA·h/g gradually. Importantly, when the rate is reset back to 0.2C, the reversible capacity can remain a high value of 592.1 mA·h/g without obvious capacity loss. The excellent rate performance of the RFCS/Se-50 electrode may be attributed not only to the appropriate distribution of Se, but to the proper framework of RFCS which can facilitate the transport of electrons and ions upon cycling. To further verify the cycling stability of RFCS/Se-50 electrode, the cell was tested at a high current density of 2C for Li–Se batteries (Fig. 7(e)). After 1000 cycles, the RFCS/Se-50 electrode can even maintain a high reversible capacity of 411.4 mA·h/g. Hence, the polyporous structured monodisperse carbon sphere as a cathode material guarantees the stable cycling performance of RFCS/Se electrode for Li–Se batteries.

4 Conclusions

1) The novel resorcinol–formaldehyde resins derived monodisperse spheres (RFCS) were prepared through an economical template-free process and chemical activation. With a further melting diffusion method, the RFCS/Se composite was obtained.

2) The abundant small pores inside the RFCS

provide a strong adsorption capacity with the attachment of selenium effectively. Without any heteroatom (nitrogen) doped, the RFCS/Se electrode still demonstrates a relatively high electrical conductivity of selenium and facilitates the transport of electrons and ions.

3) Owing to the stable structure of spherical carbon framework and the molecular conversion upon electrochemical cycling, the RFCS/Se-50 electrode exhibits good rate capability and excellent cycling stability.

References

- [1] ELLIS B L, LEE K T, NAZAR L F. Positive electrode materials for Li-ion and Li-batteries [J]. *Chemistry of Materials*, 2010, 22(3): 691–714.
- [2] CHEN Ze-hua, MA Yi-zhu, MA Peng-cheng, CAO Jian-liang, WANG Yan, SUN Guang, WANG Xiao-dong, BALA H, ZHANG Chuan-xiang, ZHANG Zhan-ying. Synthesis and characterization of ϵ -VOPO₄ nanosheets for secondary lithium-ion battery cathode [J]. *Transactions of Nonferrous Metals Society of China*, 2017, 27(2): 377–381.
- [3] GUAN Xiao-mei, LI Guo-jun, LI Chun-yang, REN Rui-ming. Synthesis of porous nano/micro structured LiFePO₄/C cathode materials for lithium-ion batteries by spray-drying method [J]. *Transactions of Nonferrous Metals Society of China*, 2017, 27(1): 141–147.
- [4] JI Xiu-lei, LEE K T, NAZAR L F. A highly ordered nanostructured carbon-sulphur cathode for lithium-sulphur batteries [J]. *Nature Materials*, 2009, 8(6): 500–506.
- [5] YIN Li-chao, WANG Jiu-lin, LIN Feng-jiao, YANG Jun, NULI Y. Polyacrylonitrile/graphene composite as a precursor to a sulfur-based cathode material for high-rate rechargeable Li–S batteries [J]. *Energy & Environmental Science*, 2012, 5(5): 6966–6972.
- [6] ZHANG Chao-feng, WU Hao-bin, YUAN Chang-zhou, GUO Zai-ping, XIONG Wen-lou. Confining sulfur in double-shelled hollow carbon spheres for lithium-sulfur batteries [J]. *Angewandte Chemie International Edition*, 2013, 44(2): 9592–9595.
- [7] WANG Xi-wen, ZHANG Zhi-an, QU Yao-hui, WANG Guan-chao, LAI Yan-qing, LI Jie. Solution-based synthesis of multi-walled carbon nanotube/selenium composites for high performance lithium–selenium battery [J]. *Journal of Power Sources*, 2015, 287: 247–252.
- [8] LIU Li-li, HOU Yu-yang, WU Xiong-wei, XIAO Shi-ying, CHANG Zheng, YANG Ya-qiong, WU Yu-ping. Nanoporous selenium as a cathode material for rechargeable lithium-selenium batteries [J]. *Chemical Communications*, 2013, 49(98): 11515–11517.
- [9] YUAN Xin-hai, CHEN Bing-wei, WU Xiong-wei, MO Jun, LIU Zai-chun, HU Zheng-yong, LIU Zhong-hua, ZHOU Chun-jiao, YANG Hai-jun, WU Yu-ping. An aqueous asymmetric supercapacitor based on activated carbon and tungsten trioxide nanowire electrodes [J]. *Chinese Journal of Chemistry*, 2017, 35(1): 61–66.
- [10] CHANG Zheng, WANG Xu-jiong, YANG Ya-qiong, GAO Jie, LI Min-xia, LIU Li-li, WU Yu-ping. Rechargeable Li//Br battery: A promising platform for post lithium ion batteries [J]. *Journal of Materials Chemistry A*, 2014, 2(45): 19444–19450.
- [11] YANG Chun-peng, XIN Sen, YIN Ya-xia, YE Huan, ZHANG Juan, GUO Yu-guo. An advanced selenium–carbon cathode for rechargeable lithium-selenium batteries [J]. *Angewandte Chemie International Edition*, 2013, 52(32): 8363–8367.

- [12] YANG Chun-peng, YIN Ya-Xia, GUO Yu-guo. Elemental selenium for electrochemical energy storage [J]. *Journal of Physical Chemistry Letters*, 2015, 6(2): 256–266.
- [13] LIU Lei, WEI Yan-ju, ZHANG Chuan-fang, ZHANG Chuan, LI Xu, WANG Ji-tong, LING Li-cheng, QIAO Wen-ming, LONG Dong-hui. Enhanced electrochemical performances of mesoporous carbon microsphere/selenium composites by controlling the pore structure and nitrogen doping [J]. *Electrochimica Acta*, 2015, 153: 140–148.
- [14] ZHANG Zhi-an, JIANG Shao-feng, LAI Yan-qing, LI Jun-ming, SONG Jun-xiao, LI Jie. Selenium sulfide@mesoporous carbon aerogel composite for rechargeable lithium batteries with good electrochemical performance [J]. *Journal of Power Sources*, 2015, 284: 95–102.
- [15] QU Yao-hui, ZHANG Zhi-an, JIANG Shao-feng, WANG Xi-wen, LAI Yan-qing, LIU Ye-xiang, LI Jie. Confining selenium in nitrogen-containing hierarchical porous carbon for high-rate rechargeable lithium–selenium batteries [J]. *Journal of Materials Chemistry A*, 2014, 2(31): 12255–12261.
- [16] STOBER W, FINK A, BOHN E. Controlled growth of monodisperse silica spheres in the micron size range [J]. *Journal of Colloid and Interface Science*, 1968, 26(1): 62–69.
- [17] EVERS S, NAZAR L F. Graphene-enveloped sulfur in a one pot reaction: a cathode with good coulombic efficiency and high practical sulfur content [J]. *Chemical Communications*, 2012, 48(9): 1233–1235.
- [18] CUI Yan-jie, ABOUIMRANE A, LU Jun, BOLIN T, REN Yang, WENG Wei, SUN Cheng-jun, MARONI V A, HEALD S M, AMINE K. (De)lithiation mechanism of Li/SeS(x) (x=0–7) batteries determined by in situ synchrotron X-ray diffraction and X-ray absorption spectroscopy [J]. *Journal of the American Chemical Society*, 2013, 135(21): 8047–8056.
- [19] LIA Zhao-qiang, YIN Long-wei. MOF-derived, N-doped, hierarchically porous carbon sponges as immobilizers to confine selenium as cathodes for Li–Se batteries with superior storage capacity and perfect cycling stability [J]. *Nanoscale*, 2015, 7(21): 9597–9606.
- [20] ZHANG He, YU Fa-qi, KANG Wen-pei, SHEN Qiang. Encapsulating selenium into macro-/micro-porous biochar-based framework for high-performance lithium–selenium batteries [J]. *Carbon*, 2015, 95: 354–363.
- [21] JIANG Yong, MA Xiao-jian, FENG Jin-kui, XIONG Sheng-lin. Selenium in nitrogen-doped microporous carbon spheres for high-performance lithium–selenium batteries [J]. *Journal of Materials Chemistry A*, 2015, 3(8): 4539–4546.

高性能可充式锂硒电池 多孔分散碳球/硒复合物的合成与表征

颜 军^{1,2}, 刘维芳¹, 陈 诚¹, 赵陈浩³, 刘开宇^{1,2}

1. 中南大学 化学化工学院, 长沙 410083;
2. 中南大学 镁资源高效清洁利用湖南省重点实验室, 长沙 410083;
3. 龙岩学院 化学与材料学院, 龙岩 364000

摘 要: 为了探索锂硒电池中负载硒的合适材料, 以间苯二酚-甲醛树脂作前驱体通过熔融-分散法制备多孔分散碳球/硒复合物。首先, 通过将间苯二酚-甲醛树脂碳化, 随后用氢氧化钾活化制备得到多孔分散碳球。对 3 种含有不同质量比的多孔碳球/硒复合物样品进行 XRD、拉曼光谱、扫描电镜、BET 比表面积法和元素图谱测试。结果表明, 硒在复合物样品中含量的不同会形成不同的内部结构, 硒在多孔分散碳球/硒复合物中的最佳含量为 50%, 这种复合物电极在 0.2C 的电流密度下经过 100 次循环表现出 643.9 mA·h/g 的高比容量。

关键词: 锂硒电池; 正极材料; 碳球; 溶胶凝胶法

(Edited by Bing YANG)